

# Cosmic-Ray Anisotropy from Large Scale Structure and the effect of magnetic horizons

N. Globus,<sup>1\*</sup> T. Piran,<sup>1</sup> Y. Hoffman,<sup>1</sup> E. Carlesi<sup>2</sup>, D. Pomarède<sup>3</sup>

<sup>1</sup>*Racah Institute of Physics, The Hebrew University of Jerusalem, 91904 Jerusalem, Israel*

<sup>2</sup>*Leibniz Institut für Astrophysik, An der Sternwarte 16, 14482 Potsdam, Germany*

<sup>3</sup>*Institut de Recherche sur les Lois Fondamentales de l'Univers, CEA Saclay, F-91191 Gif-sur-Yvette, France*

Released 14 December 2024

## ABSTRACT

Motivated by the  $\sim 7\%$  dipole anisotropy in the distribution of ultra-high energy cosmic-rays (UHECRs) above 8 EeV, we explore the anisotropy induced by the large scale structure, using constrained simulations of the local Universe and taking into account the effect of magnetic fields. The value of the intergalactic magnetic field (IGMF) is critical as it determines the UHECR cosmic horizon. We calculate the UHECR sky maps for different values of the IGMF variance and show the effect of the UHECR horizon on the observed anisotropy. The footprint of the local ( $\lesssim 350$  Mpc) Universe on the UHECR background, a small angular scale enhancement in the Northern Hemisphere, is seen. At 11.5 EeV (the median value of the energy bin at which the dipole has been reported), the LSS-induced dipole amplitude is  $A_1 \sim 10\%$ , for IGMF in the range [0.3-3] nG for protons, helium and nitrogen, compatible with the rms value derived from the cosmic power spectrum. However at these energies the UHECRs are also influenced by the Galactic Magnetic Field (GMF) and we discuss its effect on the LSS-induced anisotropy.

**Key words:** cosmic-rays

## 1 INTRODUCTION

The origin of the ultra-high energy cosmic-rays (UHECRs) is still unknown. To identify a source we need to know the arrival direction of the UHECRs. However, UHECRs are deflected on their way to the Earth by the intervening Galactic and intergalactic magnetic fields (GMF and IGMF, respectively). The only observed statistically significant deviation from isotropy is a large scale dipole anisotropy (Pierre Auger Collaboration 2017), of the order of a few percent, reported at  $\sim 5\sigma$  significance level for UHECR energies  $E > 8$  EeV.

We can expect that extragalactic UHECR sources follow, up to a biasing factor, the large scale structure (LSS) of the Universe. Both the energy and composition of the cosmic-rays change during the extragalactic propagation because of their interaction with the cosmological photons backgrounds (GZK effect). Moreover, contrarily to the photons, neutrinos and gravitational waves, UHECRs are deflected by the IGMF, and enter a diffusion regime after a time of a few  $D/c^2$  ( $D$  is the diffusion coefficient).

The observed UHECR dipole anisotropy is set by the size of the UHECR observable Universe. The "cosmic-ray horizon", the largest distance that the UHECR can propagate at a given energy, depends on their diffusion coefficient in the IGMF and on

their mean free path in the photons backgrounds. Different nuclei don't experience the same energy losses, and therefore, even if they have the same rigidity  $\sim E/Z$  (i.e. they behave the same way in the IGMF), they have different horizons. This situation is unique to UHECRs: different energy and nuclei species probe different distances. Therefore, it has been suggested that, at a given energy and composition, the anisotropy in the UHECR background probes the source distribution within the cosmic-ray horizon (Waxman et al. 1997). We investigate this possibility, assuming that the distribution of UHECR sources follow the LSS. We calculate the UHECR dipole anisotropy induced by the matter distribution, taking into account the diffusive propagation of the UHECRs in the IGMF. We derive the amplitude and direction of the UHECR dipole, for different IGMF values and different compositions. We then estimate the effect of the GMF on the LSS-induced UHECR anisotropy, for proton and nitrogen at 11.5 EeV.

In a previous study (Globus & Piran 2017, hereafter GP17), we derived the expected UHECR extragalactic dipole from the observed LSS density power spectrum. We found a maximum value for the rms dipole amplitude of  $\sim 8b\%$  for IGMF strength  $\geq 1$  nG, for helium and nitrogen at energies greater than 8 EeV. Here  $b$  is the bias factor, larger than unity if the UHECR sources are more clustered than the dark matter.

The novelty of our approach here is the reconstructed density field of the local Universe (Hoffman et al. 2018) based on the

\* E-mail: noemie.globus@mail.huji.ac.il

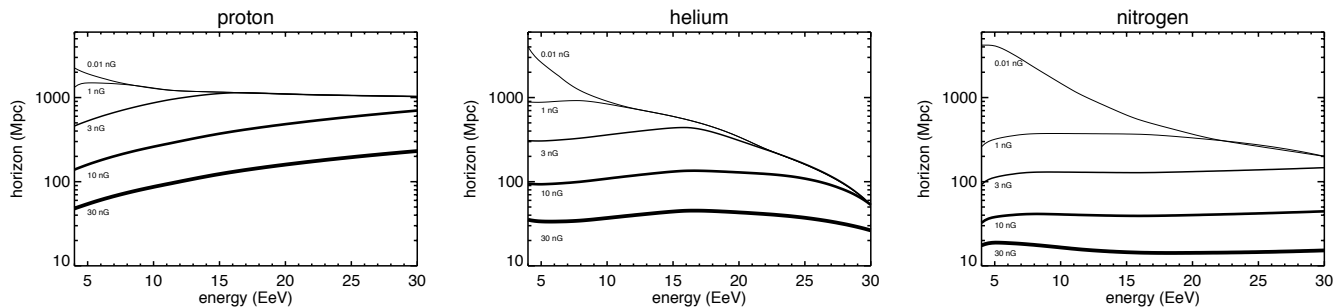


**Figure 1.** UHECR horizons as a function of the energy for different values of the IGMF.

*CosmicFlow-2* catalog of peculiar velocities to calculate sky maps of the UHECR anisotropy induced by the LSS for different UHECR horizons. A 3D view of the density field used in our calculations can be explored at this link [<https://skfb.ly/6AFxT>] where all the major overdensities of the Local Universe are shown as isosurfaces of different colors.

To derive the LSS-induced anisotropy, we consider different cosmic-ray horizons that are determined by the diffusion of UHECRs of different compositions in different IGMFs.

In this work we assume a homogeneous and purely turbulent IGMF. In reality the IGMF variance is expected to be correlated with the different structures, clusters, filaments, voids (e.g. Kotera & Lemoine 2008). This may change the propagation of the UHECRs in the field with stronger deflections within regions of stronger magnetic field and weaker ones. The overall effect might be mimicked by varying the coherence length or by more detailed simulations. However, as we are mostly interested in the dipole this would probably won't have a significant effect, as already shown by Hackstein, Vazza, Brügggen, Sorce & Gottlöber (2018) who tested different magnetogenesis models and obtain similar UHECR anisotropy for the different models. Note, however, that these authors didn't consider the GMF which, as we show later, has a significant effect on the dipole and hence must be taken into account. Note also that these authors assume a homogeneous source distribution beyond 140 Mpc, reducing the dipole for UHECRs whose horizon is larger than this distance.

The plan of the paper is as follow. We present the observations in section 2. We discuss the effects of the intergalactic magnetic fields on the UHECR horizons in section 3. In section 4 we discuss the reconstruction of the density field and the calculations of the UHECR propagation in the IGMF. We present the results in section 5. We show the effect of the GMF in section 6 and discuss our results in 7.

## 2 THE OBSERVED UHECR DIPOLE

The Pierre Auger Observatory (hereafter Auger) has measured a large-angular scale dipolar anisotropy in the distribution of the arrival directions of the ultra-high energy cosmic-rays (UHECR) at energies above 8 EeV (with a mean energy of 11.5 EeV). The dipole amplitude is  $A_1 = (6.5^{+1.3}_{-0.9})\%$  and its direction  $(l, b) = (233^\circ, -13^\circ) \pm 10^\circ$  in Galactic coordinates (Pierre Auger Collaboration 2017).

At lower energies, 4-8 EeV (with a mean 5 EeV) Auger reported a dipole amplitude  $A_1 = (2.5^{+1.0}_{-0.7})\%$  and a direction  $(l, b) =$

$(286^\circ, -32^\circ) \pm 10^\circ$  ( $\sim 50^\circ$  away from the  $> 8$  EeV dipole). However this lower energy dipole is not statistically significant.

The composition seems to be different in these two energy bins. The interpretation of the measurements of the composition-dependent<sup>1</sup> observable  $X_{\max}$  (the atmospheric depth of the air shower maximum) is as follow (Aab et al. 2017):

Above 8 EeV, the spread in the  $X_{\max}$  distribution indicates that the composition seems to be dominated by a single component (i.e. one specie dominates at a given energy), likely helium or nitrogen. Specifically, the EPOS-LHC model (Werner et al. 2006; Pierog & Werner 2009) gives nitrogen-like elements up to  $\sim 60$  EeV. At the highest energies, i.e. above 60 EeV, the model suggests a composition heavier than nitrogen (Aab et al. 2017), but due to small number statistics the uncertainties are large.

In the [4-8] EeV energy range (where the sky is compatible with isotropy) the mean value of the  $X_{\max}$  distribution indicates that the composition is dominated by lighter elements. The spread in the  $X_{\max}$  distribution indicates that there is a mixture of many components at these energies. Specifically, protons (a significant fraction, up to 50%) but also heavier nuclei seems to be present in this lower energy range.

## 3 COSMIC-RAY HORIZONS, FROM THE BALLISTIC TO THE DIFFUSIVE REGIME

The observable UHECR Universe is limited to the cosmic-ray *horizon*, i.e. the distance that a cosmic-ray, at a given energy, can propagate from its source. With no IGMF the UHECR horizon is  $d_{\text{GZK}}$ , the GZK distance at which the relevant nuclei disintegrate and a relevant proton loses its energy. For a purely turbulent IGMF, the UHECRs diffuse over a diffusion distance  $d_{\text{diff}} \sim 6D/c$  (e.g. Globus et al. 2008) where  $D$  is the diffusion coefficient.

For a Kolmogorov turbulence, the diffusion coefficient  $D$  is well approximated by a fitting function taking into account both the resonant and non-resonant diffusion regimes (Globus et al. 2008),

$$D \approx 0.03 \left( \frac{\lambda_{\text{Mpc}}^2 E_{\text{EeV}}}{Z B_{\text{nG}}} \right)^{1/3} + 0.5 \left( \frac{E_{\text{EeV}}}{Z B_{\text{nG}} \lambda_{\text{Mpc}}^{0.5}} \right)^2 \text{Mpc}^2 \text{Myr}^{-1} \quad (1)$$

where  $Z$  is the charge of the cosmic-ray,  $E_{\text{EeV}}$  is its energy measured in EeV,  $B_{\text{nG}}$  the IGMF strength in nG and  $\lambda_{\text{Mpc}}$  its coherence length in Mpc.

If  $d_{\text{diff}}$  is smaller than  $d_{\text{GZK}}$  then the horizon from which the

<sup>1</sup> It is also energy-dependent and it should be kept in mind that this dependence is not fully understood yet.

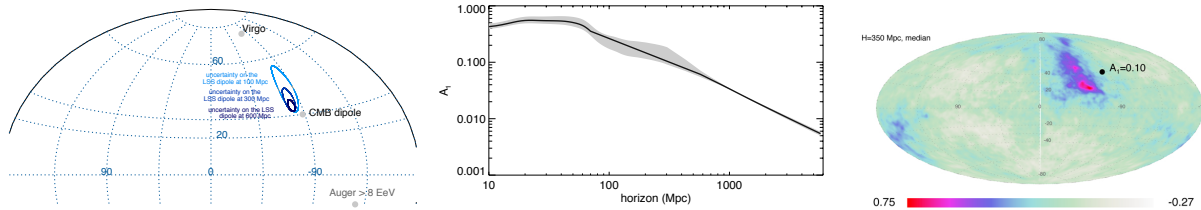


**Figure 2.** Left panel: Directions of the dipole induced by the matter distribution derived in Hoffman et al. (2018), at different depths. The QL density field is shown at the link [https://skfb.ly/6AFxT]. Middle panel: The amplitude of the dipole induced by the matter distribution at different depths. The uncertainty corresponds to the 16 and 84 percentiles of the distribution of the reconstructed density field. Right panel: A sky map, in Galactic coordinates, showing the anisotropy resulting from the integrated density field (column density) up to a maximal distance of 350 Mpc. The amplitude  $A_1$  and direction of the dipole induced by this matter distribution is indicated by a black dot.

UHECRs can reach Earth becomes:  $\sim (6Dd_{\text{GZK}}/c)^{1/2}$ . Combined the UHECR horizon is given by:

$$H(E) = \min(\sqrt{d_{\text{diff}}d_{\text{GZK}}}, d_{\text{GZK}}). \quad (2)$$

While the diffusion in the magnetic field depends just on the rigidity of the nuclei, its GZK distance depends on its type and energy. Hence different UHECRs will have different horizons even if they have the same rigidity or the same energy.

Fig. 1 depicts the horizon distance for protons, helium, nitrogen as a function of the energy for different IGMF strengths (0.01, 1, 3, 10 and 30 nG) and a maximum turbulence scale of 1 Mpc. The horizons are constant (equal to  $d_{\text{GZK}}$ ) for small magnetic fields and they decrease linearly with  $B$  for higher values.

## 4 METHODS

If the UHECR source distribution follows the LSS, its density is proportional to the matter density field  $\rho(r, \hat{e})$ . Anisotropies in the UHECR background are related to the density contrast field  $\delta(r, \hat{e}) \equiv (\rho(r, \hat{e}) - \bar{\rho})/\bar{\rho}$ , where  $\hat{e}$  is an arbitrary direction in the sky, and  $r$  is the radial distance. We begin by estimating this field.

### 4.1 The Density Field

In the standard model of cosmology, the matter density and velocity fields are closely related by the continuity equations. Hence observations of the peculiar velocities of galaxies allow for an unbiased mapping of the underlying mass distribution. The reconstruction of the density field from galaxy peculiar velocities commenced with the POTENT algorithm (Dekel et al. 1990). The more powerful and versatile Bayesian approach of the Wiener filter (WF) and constrained realizations (CRs) of Gaussian fields was applied almost a decade later to reconstruct the LSS from peculiar velocities (Zaroubi, Hoffman & Dekel 1999). The WF/CRs methodology provides a better control over the resolution of the recovered LSS and allows for extrapolation of the density and velocity fields to regions outside the data zone (e.g. the Galactic zone of avoidance). Yet, like the POTENT the WF/CRs algorithm is strictly valid only the linear regime, where deviations from the homogeneity and isotropy are small. The WF/CRs has been applied to the currently state-of-the-art CosmicFlows database of peculiar velocities (Tully, Courtois, Hoffman & Pomarède 2014; Hoffman, Pomarède, Tully & Courtois 2017, and references therein.). The WF/CRs methodology has been applied to set up constrained initial conditions for cosmological simulations, resulting with so-called constrained simulations

(for a review see Yepes, Gottlöber & Hoffman 2014; Sorce, Courtois, Gottlöber, Hoffman & Tully 2014).

The linear WF/CRs algorithm has been recently extended to the quasi-linear (QL) regime by means of constrained simulations (Hoffman et al. 2018). An ensemble of 20 cosmological simulations constrained by the CosmicFlows-2 (CF2) data (Tully et al. 2013) was constructed and used to sample the posterior distribution of the present density and velocity fields given the  $\Lambda$ CDM cosmology and the CF2 data. Taking the mean and variance over this sample provides an estimator for the present epoch QL structure of the nearby universe. The QL density field is estimated by means of the geometric mean of the ensemble of the constrained simulations and the arithmetic mean over the velocity fields provides a proxy to the QL velocity fields. The effective resolution of the QL fields is roughly 5 Mpc. It should be noted that the resolution of the individual constrained simulations is higher but the smoothing induced by the averaging process renders the resolution to  $\sim 5$  Mpc. The main effect of the the averaging process is to wash out the internal virial structure of groups and clusters.

The QL density field is calculated on a Clouds-in-Cells grid of  $512^3$  size within a periodic box of  $\sim 350$  Mpc depth. The density field beyond the box boundaries is obtained in the linear regime using a series of constrained realisations within a  $\sim 1830$  Mpc depth. At larger distances we simply assume that the Universe is homogeneous, i.e.  $\delta(r, \hat{e}) = 0$  for  $r > 1830$  Mpc. For most cases of interest this is larger than the GZK distance.

A view of this median density field is shown at [https://skfb.ly/6AFxT]. As UHECRs with different energy and composition have different horizons we show in Fig. 2 the amplitude and direction of the dipole induced by this density field at different depths with no IGMF. The uncertainty in the density field leads to an uncertainty in the dipole amplitude, which is shown in Fig. 2 by the shaded area. The uncertainty in the direction of the dipole due to the uncertainty in the distribution of matter is also shown at different depths (100, 300 and 600 Mpc). At large distances, the direction of the dipole due to the matter distribution converges to the direction of the CMB dipole. As we see later, once the horizon distance of a given UHECR is known (see Fig. 1) the overall properties of the corresponding LSS induced dipole can be read from this figure.

### 4.2 Calculation of the UHECR anisotropy

The intensity profile of a cosmic-ray source on the sky depends on the scattering properties of the particles in the IGMF. These prop-

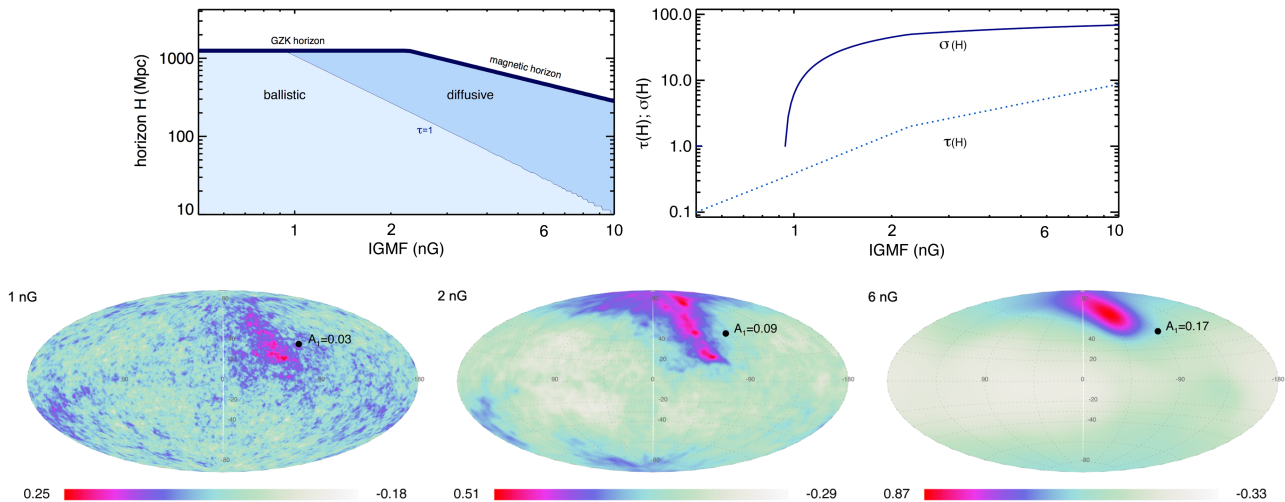


**Figure 3.** Top: left panel, the magnetic horizon  $H$  (i.e. size of the UHECR observable Universe) and the radius at which  $\tau = 1$  for 11.5 EeV protons, as a function of the IGMF. Right panel, the optical depth  $\tau$  and the angular spread  $\sigma$  of a single source at the horizon as a function of the IGMF. Lower panel: LSS-induced anisotropy for different IGMF. Three different characteristic behaviour are shown and corresponds to IGMF : 1, 2 and 6 nG. In the left sky map, all the observable Universe is in the ballistic regime, as can be seen on the upper plot. In the middle sky map, the local Universe ( $\leq 350$  Mpc) is still in the ballistic regime while the rest of the Universe is in the diffusive regime. Right sky map: only very local sources ( $\leq 30$  Mpc) are in the ballistic regime. For a LSS-induced anisotropy this corresponds to a concentration in the direction of the Virgo cluster. The amplitude  $A_1$  and direction of the dipole component are indicated by black dots. An animation showing the evolution of the anisotropy for IGMF variances from 0.01 nG to 10 nG is available in the supplementary materials.

erties depend in turn on the optical depth<sup>2</sup>

$$\tau = rc/D \quad (3)$$

where  $r$  is the distance from the source and on the typical single scattering angle, characterized by the rms value

$$\langle \delta\theta^2 \rangle \sim (\lambda_c / \beta r_L)^\kappa \langle \delta B^2 \rangle / B^2, \quad (4)$$

where  $\kappa = 2$  for  $\lambda_c \leq r_L$  and  $\kappa = -2/3$  for  $\lambda_c > r_L$  for a Kolmogorov turbulence (Kotera & Lemoine 2008). We assume strong turbulence ( $\langle \delta B^2 \rangle / B^2 = 1$ ).

Once  $\tau$  and  $\langle \cos(\delta\theta) \rangle$  are known, the image of the source is calculated as follow: using  $\tau$  and  $\langle \cos(\delta\theta) \rangle$ , we estimate the rms angular width of the source  $\sigma(\tau, \langle \cos(\delta\theta) \rangle) = \sigma(r, D)$  (Narasimhan & Nayar 2003). We then approximate the angular distribution of the cosmic-rays from this source as a Gaussian with this width. This Gaussian,  $G$ , characterizes for a given shell at a distance  $r$  and a diffusion coefficient  $D$ , the angular distribution on Earth from sources on this shell. Integrating over all distances up to the cosmic-ray horizon we obtain

$$I_i(\hat{e}, D_i(E)) = \int_0^{H_i(E)} \int_{\Omega'} \delta(r, \hat{e}') G[\cos^{-1}(\hat{e} \cdot \hat{e}') / \sigma(r, D_i(E), \delta\theta_i)] dr d\Omega' \quad (5)$$

where  $\delta(r, \hat{e}')$  is the source intensity (we assume it is proportional to the density contrast),  $D_i(E)$  is the diffusion coefficient,  $\delta\theta_i$  is the rms scattering angle and  $H_i(E)$  the cosmic-ray horizon, where the scalar  $i$  denotes the particle species.

At a given energy  $E$ , the cosmic ray horizon, the diffusion coefficient and the single scattering angle depends on the nature of the particles (section 2) and on the IGMF parameters ( $B, \lambda_c$ ). We

derive sky maps  $I(\hat{e}, D(E))$ , for different composition ( $Z = 1, 2, 7$ ) and IGMF values. The sky maps are shown in Galactic coordinates. We calculate the dipole moment (amplitude and direction) of each sky map.

## 5 RESULTS

### 5.1 Sky maps

Sky maps of the LSS-induced anisotropy for protons at 11.5 EeV, are shown in Fig.3. The UHECR horizon, as well as the distance at which the Universe become diffusive to cosmic-rays ( $\tau \sim 1$ ) is indicated in the upper panel. We also indicate the angular size  $\sigma(r, D(E))$  of a source located at the horizon.

First in practically all cases there is an enhancement in the direction ( $l = 310^\circ \pm 10^\circ$ ,  $b = 40^\circ \pm 25^\circ$ ). This corresponds (see Fig. 2) to a direction between the CMB dipole (the distant universe) and Virgo (the very local universe). It is interesting to note that Cen A is located at the edge of this region and that clustering has been reported at energies in this direction (Aab et al. 2015). The dipole is in this basic direction as well, but its amplitude varies among the different cases. When the UHECR horizon is large ( $> 350$  Mpc), the dipole direction converges to the direction of the CMB dipole.

Beyond this basic structure one can see three different characteristic behaviours in this figure:

1) In cases that magnetic diffusion is unimportant and  $d_{\text{GZK}}$  is large, the effective horizon is of order Gpc. UHECR propagation is ballistic and the anisotropy map is granular with a significant small scale structure. The common enhancement in the direction of ( $l = 310^\circ \pm 10^\circ$ ,  $b = 40^\circ \pm 25^\circ$ ) appears here as well. The overall magnitude of the dipole is small, of order of a 3% percent.

2) The second case correspond to a situation in which the magnetic diffusion is important. One first notice that the anisotropy maps are smoother now, because of the enhanced diffusion. In this

<sup>2</sup> This optical depth is not the optical depth for a single scattering. Instead it corresponds to a large angle scattering  $\langle \delta\theta^2 \rangle \sim 1$  that arises from multiple small scatterings.

case we can see the effect of the structure of "local" (i.e. few hundred Mpc) Universe. Corresponding to the LSS dipole amplitude shown in Fig. 2 the dipole amplitude is of order 10%, compatible with the rms dipole amplitude (GP17) and with the observed dipole.

3) The third case correspond to a situation in which most sources are in the diffusion regime. The dipole amplitude is large, of order of 20%.

We calculated sky maps for protons, nitrogen and silicon at 50 EeV in 1 nG IGMF. Protons at 50 EeV have a sky map similar to the left one in the figure 3 and nitrogen and silicon to the middle one.

The transitions between the three cases take place at different values of the IGMF for different energy and nuclei specie. The diffusion coefficient, eq.1, as well as the single scattering angle, eq.4, scales with the particle rigidity. The UHECR horizon, equation 2, depends on the type of nuclei. For a given specie and IGMF values, we can determine the angular spread of a source at the horizon  $\sigma_H$ . The first sky map corresponds to  $\sigma_H \sim 1^\circ$ , the second to  $\sigma_H \sim 45^\circ$ , the third one to  $\sigma_H \sim 90^\circ$ .

## 5.2 The LSS-induced dipole anisotropy

There are two effects that controls the dipole amplitude: first, the horizon size (a smaller horizon implies a larger dipole) and second, the diffusion in the IGMF (a smaller diffusion coefficient implies a smaller dipole amplitude).

1) When the IGMF is negligible, the amplitude of the dipole anisotropy is *constant*, set by the GZK distance.

2) When the IGMF starts to become significant, the amplitude of the dipole *increases* because the dominant contribution to the dipole is given by sources located at  $r \lesssim 350$  Mpc that are still in the ballistic regime. Therefore the effect of decreasing the horizon size is dominant over the diffusion effect.

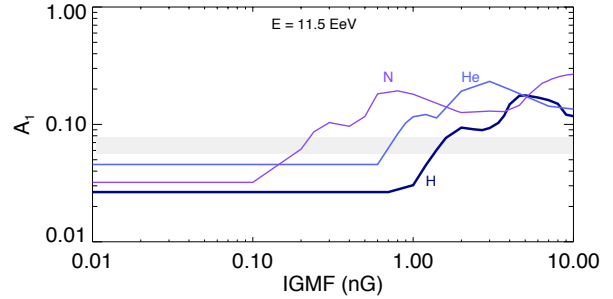
3) For IGMF large enough, the local Universe ( $r \lesssim 350$  Mpc) enters the diffusion regime and therefore the amplitude of the dipole *decreases* because the dominant effect is the diffusion.

Fig. 4 shows the dipole amplitude for different composition at 11.5 EeV. This corresponds to the median value of the energy at which the dipole has been reported. At 11.5 EeV the composition seems to be dominated by nitrogen (see section 2). We find an amplitude of  $\sim 10\%$  for nitrogen for an IGMF  $\sim 0.3$  nG.

Fig. 5 shows the dipole amplitude at 5 EeV. The lower energy bin seems to be dominated by light elements (see section 2). For an IGMF of 0.3 nG we find a dipole amplitude for protons smaller than 2%, compatible with the observed value.

## 6 THE EFFECT OF THE GALACTIC MAGNETIC FIELD

The GMF has a lensing effect that leads to a distortion of the fluctuations of the extragalactic UHECR background. This effect depends on the position of the source in the sky and on the particle's rigidity. At rigidities  $\gtrsim 10$  EV, UHECRs are deflected significantly by the GMF (Farrar 2016). To reconstruct the sky maps after GMF propagation, we use the antiparticle tracing method (Thielheim & Langhoff 1968). We back-propagate  $2 \cdot 10^5$  anti-protons and anti-nitrogen in the GMF magnetic field of Jansson & Farrar (2012), at a the energy 11.5 EeV. The initial directions  $(l_{in}, b_{in})$  of the velocity vectors are uniformly distributed. For each  $(l_{in}, b_{in})$  there is a corresponding direction outside the Galaxy,  $(l_{out}, b_{out})$ , where the trajectory of the particle becomes ballistic. Each trajectory is assigned



**Figure 4.** LSS-induced dipole at 11.5 EeV for different composition. While we use the mean of the 20 realizations here, the uncertainty on the LSS-induced dipole can be read on Fig. 2. The observed amplitude with its uncertainty is figured by the shaded area.

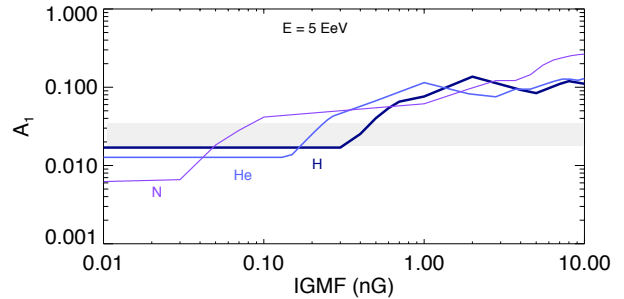


**Figure 5.** LSS-induced dipole at 5 EeV for different composition. The observed amplitude with its uncertainty is figured by the shaded area.

an extragalactic intensity  $I(l_{out}, b_{out})$  based on the previous calculations. We use  $6^\circ$  pixels for the sky maps on Earth. For each pixel on Earth, we assign the average extragalactic intensity arriving to that pixel. The resolution of  $6^\circ$  on Earth is sufficient to indicate how the extragalactic anisotropy is deformed by the GMF.

As an illustration of the effect of the GMF, we show in Fig.6 examples of sky maps, using the GMF model of Jansson & Farrar (2012), of a LSS-induced anisotropy for protons and nitrogen at 11.5 EeV. At smaller rigidities, the image is a combined effect of the IGMF and GMF, as can be seen for nitrogen for two different values of the IGMF, 0.2 and 3 nG.

The GMF smooths the sky map but also changes the direction of the dipole. The dipole moment of the sky map is moved from the Northern to the Southern hemisphere, and it is not far from the direction observed by Auger. The effect of changing the direction of the anisotropy is due to the large scale regular component of the GMF, while the smoothing is due to the turbulent component of the GMF.

## 7 DISCUSSION

We calculated the LSS-induced UHECR anisotropy, assuming that the source density is proportional to the matter density  $\rho$ . The novelty is to use constrained simulations from Hoffman et al. (2018) which provide an estimate of the local cosmic density field up to  $\sim 350$  Mpc. We developed an original approach to be able to calculate the sky maps for different IGMFs and discussed the effect of magnetic horizons on the UHECR anisotropy.

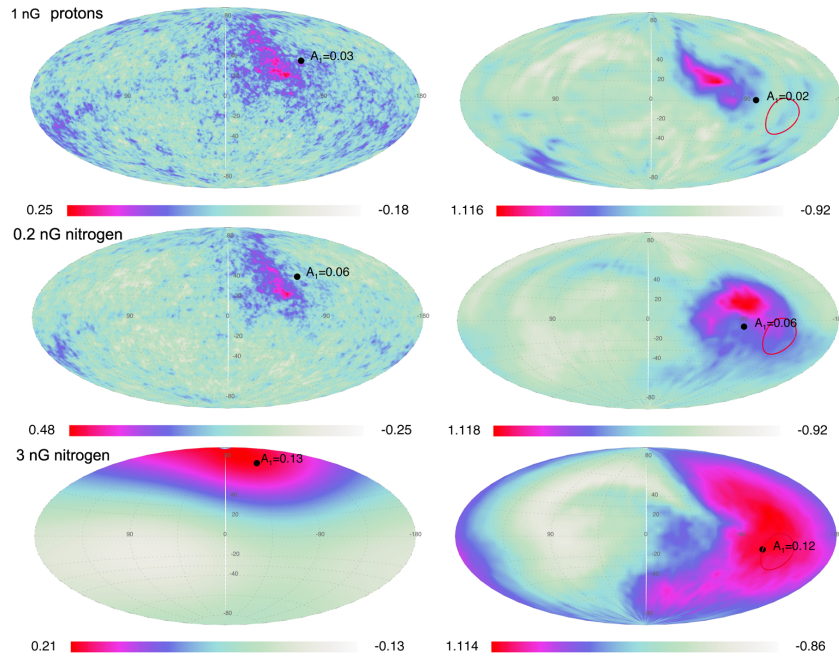


**Figure 6.** Sky maps, in Galactic coordinates, of the LSS-induced UHECR anisotropy taking into account the effect of the Galactic magnetic field of Jansson & Farrar (2012). Left, from top to bottom: the LSS-induced UHECR anisotropy for protons at 11.5 EeV in 1 nG IGMF, nitrogen in 0.2 and 3 nG IGMF respectively. Right: the anisotropy after reconstruction by the GMF of Jansson & Farrar (2012). The amplitude  $A_1$  and direction of the dipole are marked by the black dot. The observed Auger dipole direction is figured by the red circle.

With the density field of the local Universe, we recover a dipole amplitude of the same order as the rms value (GP17),  $A_1 \sim 0.1$ , for IGMF in the range [0.3–3] nG for 11.5 EeV protons, helium and nitrogen. We recall that this energy is the median value of the energy bin at which the dipole has been reported. Hoffman et al. (2018) calculated the bias relation between the matter and the density field,  $\rho_g = (\rho/\bar{\rho})^b$ , with  $b = 1.74 \pm 0.13$  for the luminosity density field derived from the compilation of the 2M++ redshift survey of galaxies (Carrick, Turnbull, Lavaux & Hudson 2015). We opted here to make the simplest assumption that the intensity of the UHECR sources follows the mass distribution. Relaxing this assumption and allowing for a linear bias factor implies that the results quoted here about the anisotropy need to be multiplied by this bias factor.

The anisotropy induced by the LSS presents small-scale structures. If protons were dominating at 11.5 EeV, a proton anisotropy would not be significantly altered by the GMF (e.g. Farrar 2016). It is interesting to note that the LSS-induced anisotropy presents an enhancement which is not far from the Cen A direction ( $l = 310^\circ$ ,  $b = 20^\circ$ ), and that a clustering was already reported in that direction by Auger (Aab et al. 2015). If nitrogen is dominating at 11.5 EeV, then the rigidity is smaller. For an IGMF of a few nG, we obtain a large scale angular anisotropy (well represented by a dipole) in the Virgo direction. Our preliminary considerations of the GMF suggest that it deflects the LSS-induced dipole towards the direction observed by Auger.

While we have presented here calculations only for a single value of the energy, a full parametric analysis is planned in a further paper to better understand the effect of varying the IGMF and GMF parameters for a given evolution of the composition with energy.

Planning and Budgeting Committee, the Israel Science Foundation (grant 1829/12), and an advanced ERC grant TRex. YH was supported by an ISF grant 1013/12. We thank the Red Española de Supercomputación for granting us computing time in the Marenstrum Supercomputer at the BSC-CNS where the simulations used for this paper have been performed.

## REFERENCES

- Pierre Auger Collaboration, Aab, A., Abreu, P., et al. 2017, *Science*, 357, 1266
- Aab A. [Pierre Auger Collaboration] The Pierre Auger Observatory: Contributions to the 34th International Cosmic Ray Conference, Proc. 34th ICRC, The Hague, The Netherlands
- Aab, A., Abreu, P., Aglietta, M., et al. 2017, *JCAP*, 4, 038
- Carrick J., Turnbull S. J., Lavaux G., Hudson M. J., 2015, *MNRAS*, 450, 317
- Dekel, A., Bertschinger, E., & Faber, S. M. 1990, *ApJ*, 364, 349
- Farrar, G. R. 2016, *IAU Focus Meeting*, 29, 723
- Globus, N., Allard, D., Parizot, E., 2008, *A&A*, 479, 97
- Globus, N., & Piran, T. 2017, *ApJL*, 850, L25
- Hackstein S., Vazza F., Brüggén M., Sorce J. G., Gottlöber S., 2018, *MNRAS*, 475, 2519
- Hoffman, Y. and Carlesi, E. and Pomarède, D. and Tully, R. B. and Courtois, H. M. and Gottlöber, S. and Libeskind, N. I. and Sorce, J. G. and Yepes, G., 2018, *Nature Astronomy* (arXiv 1807.03724)
- Hoffman Y., Pomarède D., Tully R. B., Courtois H. M., 2017, *Nature Astronomy*, 1, 36
- Jansson, R. & Farrar, G. R., 2012, *ApJ*, 757, 14
- Kotera, K., & Lemoine, M. 2008, *Phys. Rev. D.*, 77, 123003
- S. G. Narasimhan and S. K. Nayar. Shedding light on the weather.

- IEEE Computer Society Conference on Computer Vision and Pattern Recognition, USA, 1:665, 672, 2003.
- Pierog, T. & Werner, K., 2009, Nucl. Phys., Proc. Suppl. 196 102
- Sorce J. G., Courtois H. M., Gottlöber S., Hoffman Y., Tully R. B., 2014, MNRAS, 437, 3586
- Thielheim, K. O. and Langhoff, W. 1968, J. Phys. A 694
- Tully, R. B., Courtois, H. M., Dolphin, A. E., et al. 2013, ApJ, 146, 86
- Tully R. B., Courtois H., Hoffman Y., Pomarède D., 2014, Natur, 513, 71
- Waxman, E., Fisher, K. B., Piran, T., 1997, ApJ, 483, 1
- Werner, K., Liu, M. F. & Pierog, T., 2006, Phys. Rev. C74 044902
- Yepes G., Gottlöber S., Hoffman Y., 2014, NewAR, 58, 1
- Zaroubi S., Hoffman Y., Dekel A., 1999, ApJ, 520, 413